Journal of Volcanology and Geothermal Research 183 (2009) 170–182

Contents lists available at ScienceDirect

Journal of Volcanology and Geothermal Research

journal homepage: www.elsevier.com/locate/jvolgeores

Volcano spreading and fault interaction influenced by rift zone intrusions: Insights from analogue experiments analyzed with digital image correlation technique

Nicolas Le Corvec, Thomas R. Walter *

Deutsches GeoForschungsZentrum (GFZ), Potsdam, Telegrafenberg, 14473 Potsdam, Germany

ARTICLE INFO

Article history:
Received 10 November 2008
Accepted 6 February 2009
Available online 25 February 2009

Keywords:
flank instability
island volcano
rift zone intrusions
analogue model

ABSTRACT

Large volcanoes tend to be structurally unstable and subject to various forms of deformation and mass wasting. Although morphological changes associated with flank deformation and flank instability are similar on many islands, the details of the structural expression, the fault geometry and the size of the mobile flanks vary significantly. Flank instability on ocean island volcanoes is thought to be related to two principal mechanisms: gravitational spreading and intrusions into a rift zone. In this paper, we first summarize typical structures observed in nature, and then experimentally investigate structures characteristic of volcanic spreading and rift zone intrusions, in order to better understand the interplay of these two mechanisms. We reproduced unstable, intruding and deforming volcanic flanks in a sand-box and systematically studied faults developing during (i) gravitational spreading, (ii) rift zone intrusion, and (iii) combined spreading and intrusion. We recorded the experiments with a digital camera and measured deformation by applying a digital image correlation technique. This enables us to study high resolution strain fields, locate faults and analyze their related activities. The end-member models show that typical spreading structures are listric normal faults, whereas typical rift zone intrusion structures include a graben at the surface and a subhorizontal detachment at depth. Concurrent or alternating simulations of spreading and rift zone intrusions reveal the interplay of the developed faults; some are hindered while others are more encouraged to slip. For instance, while the pure spreading end-member promotes internal faulting within the unstable flank, the occurrence of rift zone intrusions hinders this type of faulting and hence may even stabilize part of the volcanic flank. We apply this understanding to Kilauea (Hawaii) and Piton de la Fournaise (La Réunion) in an attempt to better identify the related mechanisms of intrusions, flank instability and sector collapse. Important implications arise for geological and geophysical field data, such as seismicity or geodetic measurements.

1. Introduction

The architectures of large volcano edifices, especially volcanic islands, are often thought to be governed by episodes of construction and destruction. Edifice construction during magmatic activity is commonly associated with multiple intrusions and dike complexes emplaced along rift zones (Walker, 1987). Edifice destruction, in turn, occurs by various types and processes of mass wasting, including flank spreading and sector collapses (Borgia and Treves, 1992). Examples of pronounced rift zone intrusions and gravitational spreading are found on the Hawaiian Islands, La Réunion, the Canary and Madeira archipelagos, and have allowed researchers to explore the dynamics of deformation and structural interaction in the past decades. Rift zone intrusions and gravitational spreading are both found to be associated with flank movements, so their relative influences on the structural evolution of a volcano edifice are difficult to differentiate (Swanson et al., 1976).

Rift zone intrusions and gravitational spreading are thought to be coupled: the process of gravitational spreading may influence the interior stress field of a volcano edifice (Borgia and Treves, 1992), while the occurrence and geometry of dike intrusions in rift zones strongly depend on the surrounding stress field (Rubin, 1992). Forceful intrusions of dikes into a rift zone are associated with a stress change that may be associated with earthquakes and affect flank instability and gravitational spreading (Swanson et al., 1976; Rubin and Gillard, 1998; Delaney and Denlinger, 1999). Nakamura suggested that gravitational spreading may lead to a stress distribution that traps dikes within the rift zone and thus sustain the rifting process, and vice versa (Nakamura, 1980). Understanding the structural condition of volcano instability thus also requires understanding the coupling between intrusions and flank movement.

In this paper, we first summarize expressions of deformation on volcanic islands common for gravitational spreading and rift zone intrusions, and discuss possible feedback mechanisms. We illustrate this for the ocean island volcanoes of Kilauea (Hawaii) and Piton de la

* Corresponding author.
E-mail addresses: lecorvec@gfz-potsdam.de (N. Le Corvec), twalter@gfz-potsdam.de (T.R. Walter).

0377-0273/$ – see front matter © 2009 Elsevier B.V. All rights reserved.
doi:10.1016/j.jvolgeores.2009.02.006

Fournaise (La Réunion), because these are among the best studied active volcanoes and serve as type-examples. The second part concerns new analogue experiments in which we systematically simulate the conditions of two end-members: gravitational spreading and rift zone intrusions. Then we jointly simulate both mechanisms in order to examine their coupling processes. The experiments show that zones of shear localization within unstable flanks characterize the geometry and location of both gravitational spreading and intrusion events.

2. Rift zone intrusions and gravitational spreading

Volcanoes that show pronounced intrusive growth are susceptible to structural collapse and deformation associated with gravitational spreading; processes that are detailed below.

2.1. Rift zone intrusions

Most island shield volcanoes are marked by pronounced sheet-like intrusions that form rift zones (Walker, 1992). These are generally confined to large volcano edifices, and their dimensions and dynamics should not be confused with rifts typical of divergent plate margins, such as those found on Iceland (Rubin, 1990). Ocean island edifice rift zones are characterized by elongated zones encompassing dilatational cracks, faults and eruptive fissure vents at the volcano surface in response to the repeated emplacement of preferably oriented dikes at depth (Walker, 2000). The lengths and thicknesses of ocean island rift zones vary from a few kilometers to many tens of kilometers (Carracedo, 2000), and their orientations are controlled by a crustal stress field that (in case of intra-plate ocean islands) mainly depends on the load of the edifice in which they grow (Fiske and Jackson, 1972; Binard et al., 1991; Michon et al., 2007; Got et al., 2008). This means that many dike intrusions may follow preferred paths, with dike thicknesses that typically range from few decimeters to meter size (Walker, 1987; Walter and Schmincke, 2002; Letourneur et al., 2008). Each dike, as well as the summation of many dikes in a rift zone, is thought to be associated with lateral widening of the adjacent rock mass (Swanson et al., 1976). Geodetic and seismic data confirm that rift zone intrusions compress and steepen the volcano flank and lead to an increase in the flank seismicity and acceleration of flank movement (Dvorak, 1994). Some other dike intrusions, however, appear to have the opposite effect by decreasing seismicity and stabilizing the flank (Delaney and Denlinger, 1999).

2.2. Gravitational spreading

Gravitational spreading is essentially driven by gravity, and is thus thought to be mainly controlled by the morphology of a growing volcano (Nakamura, 1980; Dieterich, 1988; Merle and Borgia, 1996; Delcamp et al., 2008). The process of flank movement during gravitational spreading may be facilitated by weak materials inside the volcano. These could include hot cumulates deep along the rift systems (Clague and Denlinger, 1994; Johnson, 1995), hydrothermally- or structurally-altered materials within the edifice (Walter and Schmincke, 2002; Oehler et al., 2005), or soft pre-volcanic marine sediments at the base of the volcano, as are found below many ocean islands (Nakamura, 1980; deVoogd et al., 1999).

The structures associated with gravitational spreading have been extensively studied in numerical and physical models, considering simply-shaped volcano edifices (partly) situated on top of a weak rock type that serves as a decollement (Borgia, 1994; Merle and Borgia, 1996; van Wyk de Vries and Matela, 1998; Oehler et al., 2005; Delcamp et al., 2008). In a common scenario, a subhorizontal decollement fault at depth allows lateral movement of the flank, and is connected to one or more listric and subvertical faults that may have a normal and/or strike-slip component of motion in plan view. In ocean islands, however, such structures are often rarely visible in the field and hidden under water. The most common type of faults observed in the field is normal faulting near the headwall of the spreading flank (Mitchell, 1998; Lipman et al., 2006). Due to the lack of data on ocean islands, the fault geometry typical of gravitational spreading is not well understood, and field evidence agrees with three very different types of faulting (Walker, 1988, Borgia et al., 2000; Lipman et al., 2006). As summarized (Morgan and Clague, 2003) in Fig. 1, these are A) slump-type structures controlled by a shallowly-dipping fault affecting a superficial part of the volcanic flank, B) deep-reaching listric normal faults that also affect the deep flank, and C) horizontal slip and coherent block movement along a decollement fault.

2.3. Feedback between rift zone intrusions and gravitational spreading

Rifting and gravitational spreading are thought to be coupled processes acting together in many volcanic islands – an idea that is supported by field evidence, seismic, and geodetic data, analogue and numerical modeling (Fiske and Jackson, 1972; Swanson et al., 1976; Lipman, 1980, Dieterich, 1988). The interaction mode, however, including the structural feedback of faults and their linkage, is still debated. Several researchers (Moore and Krivoy, 1964; Delaney et al., 1998; Owen et al., 2000; Walter et al., 2006; Desmarais and Segall, 2007) have suggested that the dynamics of dike intrusions and flank displacement on many volcanic islands are governed by gravitational slumping of the flank, which causes the rift to widen and to be in part passively intruded (cf. (Moore and Krivoy 1964; Delaney et al., 1998; Owen et al., 2000; Walter and Amelung, 2006; Walter et al., 2006;

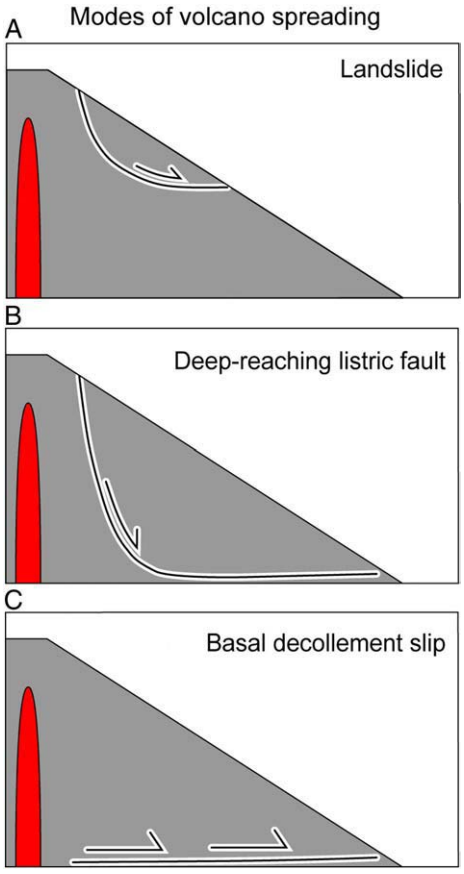

Fig. 1. Spreading types suggested to explain observed deformation and structures at ocean island volcanoes. Cross-section sketches showing a volcanic flank (in grey), a rift zone (in red), and the main structural architectures discussed in the literature, that are A) a shallow landslide, B) a deep-reaching listric fault, C) a basal decollement slip. Compiled and modified from studies at Hawaii, after Walker (1988), Borgia et al. (2000) and Morgan and Clague, (2003).

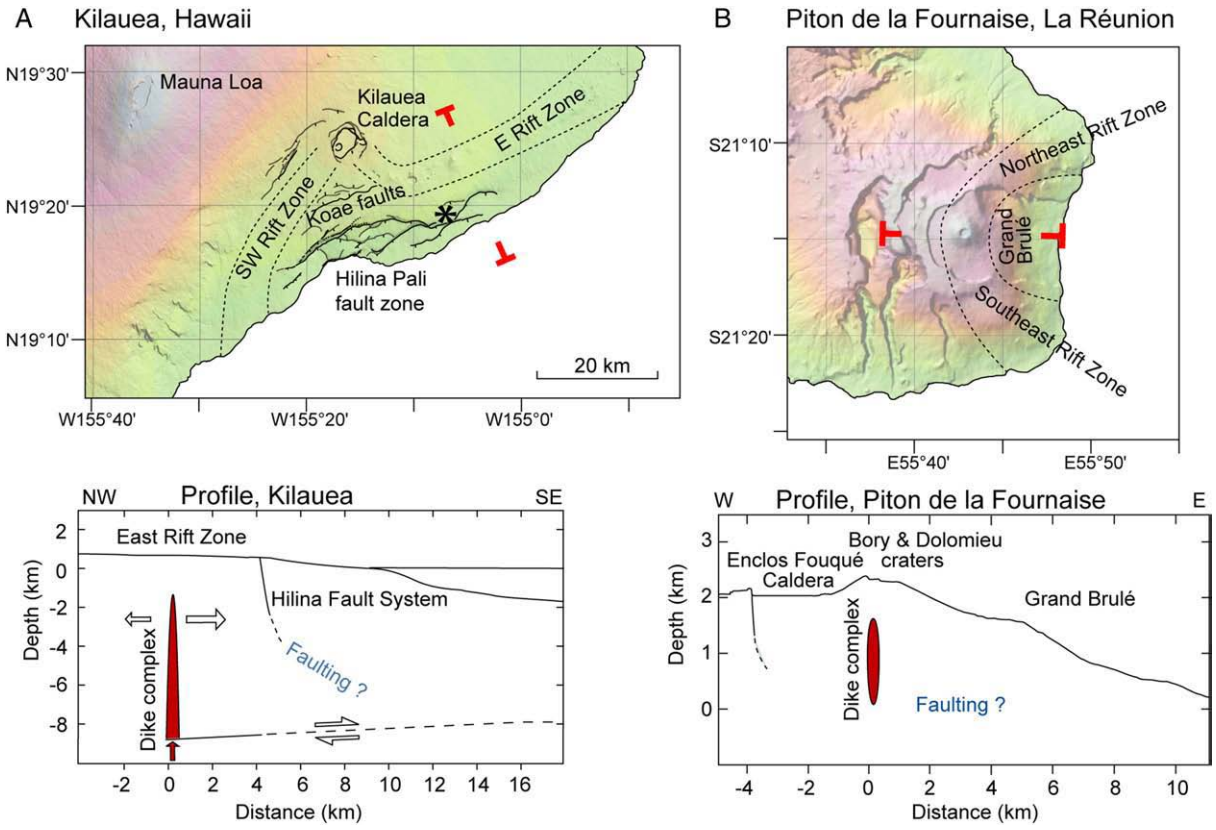

Fig. 2. Spreading and rifting flanks of Kilauea (A) and Piton de la Fournaise (B) showing intrusion and possible zone of faulting. Map view shows the locations of active rift zones (dashed lines) and selected fault systems within the rift zone (black lines). The star represents the Panau triangulation station at Kilauea volcano. Red bars indicate locations of cross section shown below the map views, distances are indicated in kilometers. At Kilauea volcano, the Koae faults are probably connected to the active rift zone, the continuation of the Hilina Pali fault zone in turn is not constrained. At Piton de la Fournaise, no active faulting is evident.

Desmarais and Segall, 2007). Geodetic data, however, suggest that magma intrusions are forceful and increase flank movements and the pressure in the rift zone. This structural complexity is summarized in the following for what are probably the best-studied case examples, Kilauea (Hawaii) and Piton de la Fournaise (La Réunion).

3. Case studies

Kilauea and Piton de la Fournaise both have pronounced rift zones, and are subject to continuous or episodic flank spreading. The expressions and structural architectures, however, are very dissimilar.

3.1. Kilauea (Fig. 2A)

Kilauea is an active basaltic volcano that forms the southeastern portion of Mauna Loa on the Big Island of Hawaii. The edifice is characterized by a summit caldera from which two narrow and well-defined rift zones radiate. The surface expression of the active East Rift zone (ERZ) is about 1.5 to 3.0 km wide and extends subaerially for 55 km. The ERZ is curved, from southeast to east to northeast, and further continues offshore to the northeast for another 70 km (Acosta et al., 2003). The surface expression of the active Southwest Rift Zone (SWRZ), in turn, is shorter and thinner, less than 1.5 km wide and about 32 km long in the southwest direction. The submarine extension of the SWRZ is poorly defined in terms of both fracture presence and topographic appearance of the flank (Acosta et al., 2003). Both rift zones are thought to be rooted close to a decollement surface at the base of Kilauea at ~9 km below sea level (Dieterich et al., 2003). The presence of this root depth and the decollement is inferred indirectly, for instance by earthquake locations (Got et al., 1994), or by inversion of geodetic observations (Segall et al., 2006). Two main fault zones have developed on land; the inward-dipping Koae fault system and the seaward-dipping Hilina fault system (Fig. 2A). These fault systems are inferred to be somehow associated with the decollement and southward displacement of the south flank of Kilauea, but the fault root depth and fault linkage to the decollement are not yet constrained by data (cf. Fig. 1).

Historical magmatic activity at Kilauea was observed until the 1950s, often as summit eruptions within the Kilauea Caldera (including Halemaumau Crater), and thereafter progressively by more rift zone fissure events occurring mainly at the ERZ. Examples of ERZ eruptions are the Kapoho 1960 eruption, the Makaopuhi 1965 eruption, which was the largest of six successive ERZ eruptions from 1961–1967, the Mauna Ulu 1969–1974 eruption, and the recent Pu'u O'o 1983 eruption, which is ongoing. According to Dzurisin and coworkers, the strong expression of the ERZ suggests that a much larger amount of magma has accumulated under this flank during the recent geologic past (Dzurisin et al., 1984). Intrusion events, mainly in the form of dike intrusions, may occur in the entire rift zone reaching from the surface to the base of the volcano (Cayol et al., 2000, Dieterich et al., 2003). Because the depth of the root zone is similar to the depth of the subhorizontal decollement plane, the ERZ and SWRZ are considered to act as upslope boundaries of the Hilina slump (Swanson et al., 1976).

Intrusive and gravitational spreading events are temporarily and spatially coupled. Repeated events of larger displacements may occur, and these affect local seismicity and thus the activity of faults and fractures within the spreading flank (Segall et al., 2006). The displacement of the southeastern flank of Kilauea is intermittently accelerated during dike injections into the rift zones, leading to compressive

stresses in the flank that are thought to be relieved during flank displacements (Duffield, 1975; Thurber and Gripp, 1988; Denlinger and Okubo, 1995; Morgan et al., 2000). Therefore, displacement of the southern Kilauea flank appears to be controlled by gravitational spreading and may be accelerated by the accumulation of magma intrusions in the rift zones. This may explain why changes in spreading velocity are associated with changes in seismic activity and fault reactivation.

3.2. Piton de la Fournaise (Fig. 2B)

Piton de la Fournaise is an active basaltic volcano that forms the southeastern portion of the island of La Réunion. Piton de la Fournaise has erupted once every 10 months for the last two centuries (Stieltjes and Moutou, 1989). Eruptions have occurred more frequently since 1998 (Longpré et al., 2007) and are fed by dikes propagating within the upper 2 km of the edifice (Lénat et al., 1989; Battaglia et al., 2005; Peltier et al., 2007). Rift zone intrusions appear to be restricted to the volcanic sector above sea level, as a deeper root of the dikes has not yet been found. The recent activity of Piton de la Fournaise is concentrated within the Enclos Fouqué depression, from which two rift zones diverge. The rift zones are organized in two corridors trending N25–30 and N120 (Michon et al., 2007). The two rift zones continue outside the caldera, curving to the northeast and southeast respectively, but do not appear to extend into the sea (deVoogd et al., 1999). The rift zones are thought to have their root at 1 km below sea level, which is <3 km below the surface (Brenguier et al., 2007). The east flank of Piton de la Fournaise is open to the sea and is the most-often discussed candidate for flank spreading, which is however very rarely observed. The apparent stability of the east flank is shown by multiple-year InSAR and ground truth geodetic observations (Briole et al., 1998; Froger et al., 2004; Fukushima et al., 2005), but it is still unclear whether the flank can remain stable over longer time periods. Gravitational spreading, lateral and vertical collapse have occurred in the past, as is clear from the morphological depression in which Piton de la Fournaise was constructed (Lénat and Labazuy, 1990; Merle and Lénat, 2003; Michon and Saint-Ange, 2008). The current eruptions and intrusions, however, are mainly associated with steepening of the upper part of the volcano close to the rift zones, while seaward flank displacements appear to occur rather seldom (Froger et al., 2004; Fukushima et al., 2005; Peltier et al., 2005) and were never clearly shown before the 2007 flank slip event (Froger et al., 2008).

Although field evidence and theoretical models suggest that rifting is occurring at Piton de la Fournaise, and gravitational spreading may intermittently occur (as in April 2007), their structural relationship in time and space is much less clear than at Kilauea.

Our new sandbox experiments help to identify the structures typical of rifting, structures typical of gravitational spreading, and how these processes may communicate with each other.

4. Experiment methodology

Analogue models are used to identify and analyze the main processes operating in natural systems at the laboratory scale, such as fault formation, interaction and propagation (Ramberg, 1981). We simulate both forceful rift intrusions into a volcanic edifice and gravitational spreading of a flank, and analyze the internal structural evolution. The aim is to determine which parameters of spreading and rifting control the observed structural deformation and finally to determine the interactions of rifting and spreading. This is a first step in understanding internal deformation due to rifting and spreading and is principally a phenomenological study. Although the experiments simulate only a very simplified version of the natural process they are able to reproduce structures similar to the natural case examples, providing insight into the basic conditions of flank-internal deformation.

4.1. Experimental setup

All experiments were performed in a sandbox (80 cm wide, 20 cm high and 10 cm deep) with panes of glass on the front and back sides. On one side, a tank with a trap-door permits its opening, so that intrusion may occur and rift zone widening is simulated at a chosen depth and width (Fig. 3). We consider a setup with a stable buttress and deforming the flank of a half topographic ridge.

The wedge-shaped flank is about 10 cm high and 20 cm wide, and is made of quartz sand, representing the crustal rock-types of the volcano edifice. A 0.5 cm thick layer underneath this “volcano flank” corresponds to syn-volcanic deposits, beneath which another layer 0.5 cm thick corresponds to pre-volcanic deposits.

We design three sets of experiments, with a varying influence of spreading and rifting. The first two sets are considered as end-members, while the third set is a combination of those. (A) The edifice flank is constructed on top of a weak silicone layer in order to investigate how gravitational spreading as the sole loading type affects the structural evolution of the edifice flank. (B) Intrusion of silicone “dikes” into the sand-ridge attempt to imitate forceful rift zone widening as the sole loading type. In order to achieve this we simulate intrusions at different levels by injecting silicone into different depths of the flank and observe the developing fault structures. (C) Finally, we combine the model setups and simulate rift zone intrusions occurring into a flank subjected to gravitational spreading (sets A and B) in order to investigate the relation between the two distinct dynamic and structural phenomena.

In the experiments simulating gravitational spreading (sets A and C), the basal layer is made of viscous silicone. In the experiments simulating rift zone intrusions only (set B), most of the basal layer is composed of granular material and thus of high friction. We use a tank variably filled with silicone to simulate magma overpressure. The dimensions of the silicone intrusion were controlled through a trapdoor; opening the trapdoor allowed the intrusion, whereas its closing stopped further silicone addition. The silicone intrusion orientation was artificially controlled to be vertically aligned along the half-topographic ridge axis, with the dimensions of the upper and lower limits constrained by the size of the trapdoor. Intrusions were achieved ranging from the surface

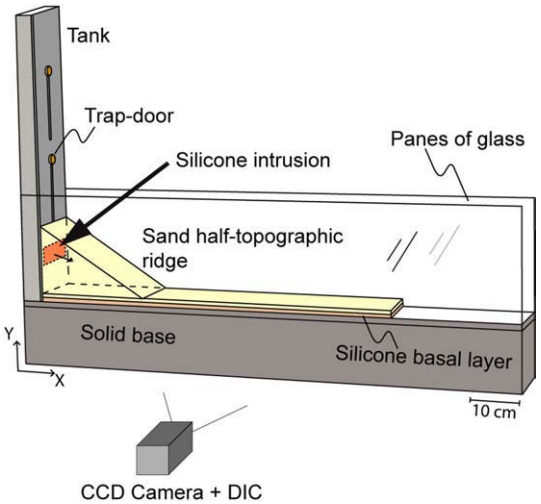

Fig. 3. Setup of the sandbox experiments. Experiments are designed in a two-dimensional setup, constrained by two parallel panes of glass distant of 10 cm. A half-topographic ridge of sand defines the volcanic flank, into which silicone intrusion is simulated from a tank (here on left side). Opening of a trap-door allows intrusion into the ridge. Basal decollement and intrusions are simulated with viscous silicone. Through a CCD-camera and digital image correlation technique (DIC) the experiment is recorded, allowing grain-size and sub-millimeter strain rate data investigations.

down to the base of the edifice with maximum thicknesses of up to 1 cm. All of this thickness is displacing the unstable part of the flank, which compares to co-intrusive displacements of an unstable flank at real volcanoes stabilized on the opposite side of the rift zone by a solid buttress. For instance, it was shown that flank movement occurring during rift zone intrusion at Hawaii and Piton de la Fournaise is mainly affecting the unbuttressed flank and hence the intrusion thickness approximates the values of flank movement (Swanson et al., 1976; Sigmundsson et al., 1999). The experimental setup allowed to record and analyze the strain localization within the flank by applying a digital image correlation technique. For this, we placed a high resolution camera at a horizontal distance of 1.5 m from the panes of glass and continuously recorded the experiments at 0.5 Hz. Thus, all results show a section through the flank recorded from the side, allowing us to investigate fault patterns in cross-section.

4.2. Dimensions and scaling

The behavior of analogue materials must be physically similar to that of natural rocks (Lohrmann et al., 2003), allowing scaled simulations of natural processes under laboratory conditions (Hubbert, 1937; Ramberg, 1981). Hawaii and La Réunion are herein considered to be geometrically similar, being 5–10 km high and 20–80 km wide (Moore and Chadwick, 1995; Lénat et al., 2001; Walter et al., 2006). The scaling ratio between the height of our experimental model ($H_{Ex} = 10$ cm) and of natural volcanoes ($H_N = 10$ km) is $H_{Ex}/H_N = 10^{-5}$ (1 cm in experiments represents approximately 1 km in nature). The dimension of an experimental volcano flank (20 cm) and of a real volcano flank (20 km) also translate to a scaling ratio of 10^{-5}, similar to the thickness of the substratum and synvolcanic sediments, which are each about 0.5 km thick (Borgia 1994; Merle and Borgia 1996; deVoogd et al., 1999; Borgia et al., 2000; Walter et al., 2006; Delcamp et al., 2008) and simulated by 0.5 cm thick substratum layers. This ratio is in agreement with Merle and Borgia (1996) to generate spreading. The height of the intrusions was tested systematically for values ranging from the base of the volcano to the surface, and covers the full observed range of intrusions from the case examples considered here. For geometric scaling, a ratio of 10^{-5} is a consistent and valid approximation (Merle and Borgia, 1996).

Quartz sand and silicone are known to scale to natural rheologies and therefore have been used by many workers and are well constrained (Schellart, 2000). The quartz sand used has a mean grain size of ~0.3 mm and is characterized by strain-hardening and strain-softening effects (Lohrmann et al., 2003), similar to natural brittle rocks. Internal friction coefficients are approximately 0.6 in both natural and experimental materials, which is necessary for the geometric similarity of the fault architecture studied in the laboratory (Schellart, 2000).

Dynamic scaling of analogue experiments is typically difficult to achieve if gravity is not scaled via a centrifuge setup (Ramberg, 1981). The densities of natural rocks (substratum ~2200 kg m^{-3}, synvolcanic sediments and volcanic rocks ~2600 kg m^{-3} (Merle and Borgia, 1996)) are in contrast to the analogue materials (silicone ~1300 kg m^{-3}, quartz sand ~1710 kg m^{-3}), and thus yield a density ratio (ρ^*) of about 0.6. Since the gravity is the same ($g^* = 1$), then to a first approximation, the stress ratio can be calculated from $\sigma^* = \rho^* g^* H^* \approx 0.6 * 10^{-5}$. This means that our model is about 0.6×10^5 times weaker than real volcanoes. Ductile material is simulated by silicone, which behaves as a Newtonian fluid at low differential stress (ten Grotenhuis et al., 2002). We use silicone to simulate a layer of the deformable substratum beneath the volcano edifice as well as for magma intrusions. We consider the viscosity of the substratum sediments to be $\mu \sim 10^{18}$ Pa s (Borgia, 1994) with the herein used silicone of $\mu \sim 10^5$ Pa s, giving a viscosity ratio for the sediments of $\mu_s^* = 10^{-13}$. As viscosity (μ), stress (σ), and time (t) ratios relate through $\mu^* = \sigma^* t^*$ (Donnadieu and Merle, 1998), the viscosity ratio for basaltic intrusions (μ_i^*) should be equal to that for sediments (μ_s^*). A basaltic intrusion has temperature-dependent viscosities, ranging from 10^1 to 10^5 Pa s (Wada, 1994). The corresponding analogue material should have a viscosity ranging from ~10^{-12} to ~10^{-8} Pa s.

Thus, our models are geometrically scaled following the principles discussed by Ramberg (1981) (Borgia et al., 2000). The viscosity, velocity, and time factors, however, are not directly comparable to spreading or rift zone intrusions; hence the herein presented relation between the influence of gravitational spreading and intrusion has to be considered qualitatively (Merle et al., 1996; Roche et al., 2000). In the following we therefore show our time-dependent strain-rate studies in normalized plots, and focus the study on the well-scaled development of brittle fractures and their interplay.

4.3. Data acquisition

Accurate recording and data acquisition of analogue experiments have significantly improved during the past years. Newer techniques include optical methods to detect topography using the double scan technique (Grujic et al., 2002), digital photogrammetry (Donnadieu et al., 2003) and particle image velocimetry (Adrian, 2005). In this work, we apply a digital image correlation technique (DIC) that provides precise measures of the velocity and displacement of laboratory flow experiments and deformation systems (Adam et al., 2005). The DIC method, developed for high-resolution 2D strain monitoring studies, is a non-intrusive optical method useful for visualizing non-linear flow and deformation. In experiments using granular materials, the DIC allows high-resolution displacement detection at the scale of individual sand grains (White et al., 2001). The temporal resolution is limited by computer components, such as the camera frame rate, data transfer speed and storage capacity. For calibration, we first recorded a plate with 2-cm equidistant cross marks in order to calibrate the entire experimental viewing field and correct any CCD-camera specific distortion (Adam et al., 2005). We then recorded the experiments with the same camera equipment at an interval of 0.5 Hz (Fig. 4A). Data processing was performed using the software package StrainMaster (LaVision, 2002), in order to calibrate and to retrieve tensors of incremental deformation. In the camera coordinate system, the *X*- and *Y*-axes describe the viewing field and the *Z*-axis is aligned with the optical axis. Here, we obtained the incremental displacement field composed of the horizontal (Vx) and vertical (Vy) vector fields within a stable reference system. The vector field we used to further analyze the strain rates (Fig. 4B). By subtracting the two incremental shear strains *Eyx–Exy*, we derived the incremental rotational shear around the *Z*-axis, i.e. *rot-Z*. Thus, the normalized rotation as a function of time can be given by the percentage of incremental rotational shear *rot-Z*, and will be used in our experiments to locate and analyze the formation of faults (Fig. 4C). In the convention used here, sinistral (i.e. counter-clockwise) rotation is shown in red (positive *rot-Z*), while dextral (i.e. clockwise) rotation at shear zones is shown in blue (negative *rot-Z*). Profiles of the percentage of rotational shear were created at the base and inside the flank for the combined experiments in order to quantify the activity of the different shear zones.

4.4. Limitations of the experiments

Model simulations, especially sandbox experiments, always require reducing the natural complexity to a small number of testable variables, and being aware of associated shortcomings, biases and side effects. In our case, limitations may be based on the simplified geometric and loading conditions considered. We simulate a volcano flank with one side buttressed by the silicone

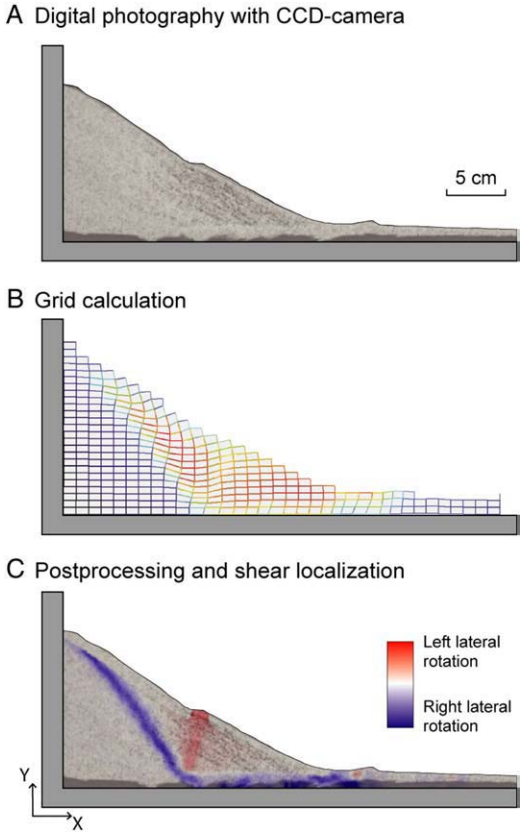

Fig. 4. Illustration of image analysis procedure. A) Raw image recorded by the CCD-camera, B) downsampled regular displacement grid showing the particle displacement in colour (red = maximum, black = minimum), C) Post processing allows to explore zones of high rotational strain in the axis *Z* of the camera's line of sight (blue = dextral shear rotation, red = sinistral shear rotation). Shear strain is always shown in a scale ±100 percent, see text for explanation.

tank and subject to no deformation. The restriction of using a half-topographic ridge is necessary in order to control the length and shape of the intrusion; however it may affect the deformation pattern of the unbuttressed flank. Moreover, in order to record the deformation in cross-section, side effects of the panes of glass cannot be excluded. We thoroughly tested similar experiments with different materials and without buttressing panes of glass, finding that the structures observed at the surface are similar to the experiments detailed herein. We therefore assume the side effects of the panes of glass to be minimal, which agrees with the findings of previous workers (Adam et al., 2005; Hoth et al., 2007). Another simplification was to simulate gravitational spreading in an already built volcano, ignoring that spreading is a progressive process acting as soon as the edifice starts to grow, associated with structural developments and resurfacing processes due to lava flows (Annen et al., 2001).

An important geometric simplification is the scale of the intrusion. While the length may show a realistic relation to the height of the edifice, the thickness commonly exceeds individual dike intrusions known from ocean island volcanoes. Dikes on ocean islands have ratios of length (kilometers) to thickness (meters) of ~1000 (Walker, 1992), whereas our experiments use a ratio of only ~10. Therefore, displacement associated with silicone intrusions shown by our experiments simulates a series of about 100 dikes, rather than a single dike injection event, which can be compared as a part of a dike complex formation (Walker, 1986). We note that we did control the geometry of the silicone intrusion. However, in nature, the geometry of magma intrusions may be significantly affected by the flank instability.

Moreover, the setup used here ignores the effects of volcano layering or other mechanical heterogeneities, as well as dipping geometries of intrusions and the decollement. As we show in the following section, although our models are simplified, important information can be extracted that helps in understanding real volcano behavior.

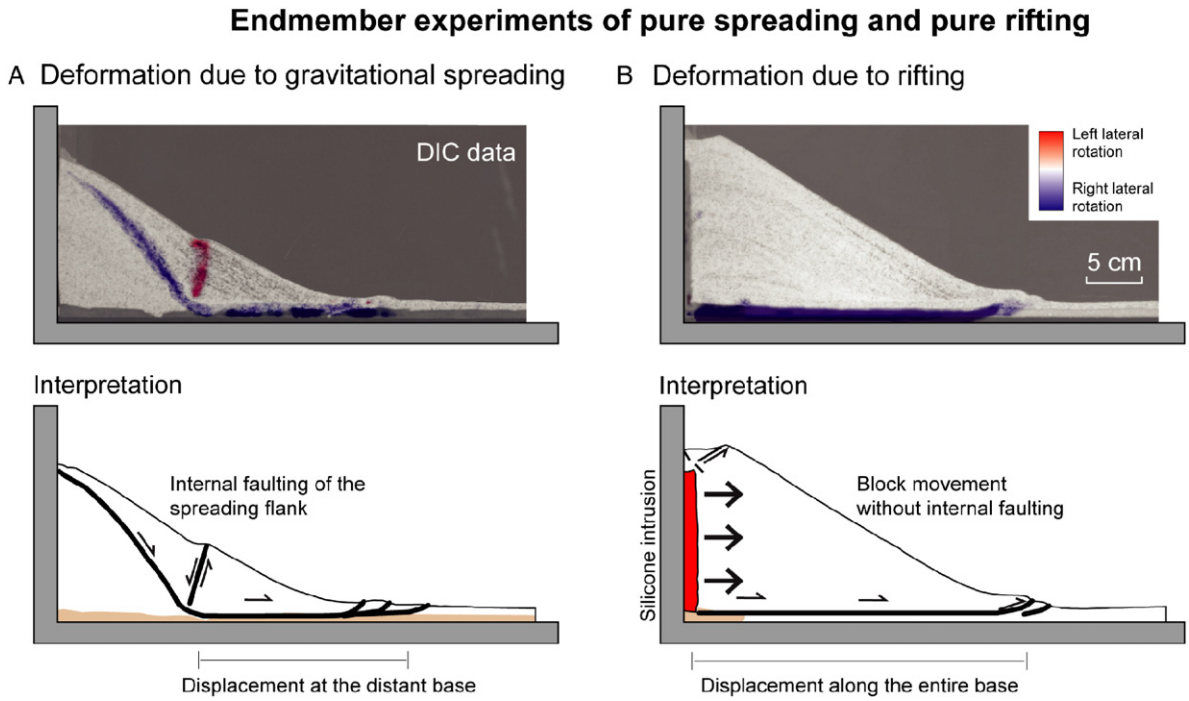

Fig. 5. Endmember experiments. Left side (A): Pure spreading is achieved through a deformable layer (silicone) situated beneath the sand flank. A listric decollement fault develops with dextral shear rotation, to which an antithetic fault is linked. At the surface, the flank is subsiding, creating a hump where the antithetic fault emerges and a thrust belt at the location where the basal decollement fault reaches the surface in the periphery. Right side (B): Pure rifting experiment is achieved by silicone intrusion from the left side by completely opening the trap door. Displacement occurs along the entire basal decollement. At the surface, the slope of the flank is near constant in this configuration, local graben subsidence occurs above the intrusion; periphery fault and thrust belt develops. Upper images show DIC results, lower images show interpretation.

5. Results

5.1. End-member models

The first set of end-member models simulates pure spreading of a volcano flank located on top of a weak decollement (Fig. 5A). Soon after edifice construction, we observe that deformation starts on the deformable (unbuttressed) flank. At the surface, outward-directed displacement occurs. The internal structure becomes visible by displaying the rotational shear, *rot-Z*, which suggests a dominant dextral shear zone (blue in Fig. 5A) located along part of the predefined silicone decollement plane. At the outer edge of the volcano flank, a set of thrust faults develops from the decollement to the surface, together with a fold and thrust region. Within the flank, the decollement is linked to a normal fault dipping ~50° outward. Spreading hence affects only the outer part of the flank, while an inner wedge-shaped part remains stable. The 50° outwardly dipping fault and the basal decollement combine to form a listric normal fault plane. At their junction, one or several antithetic faults develop, dipping 70–80° inward with sinistral rotation (red in Fig. 5A), hereafter referred to as an antithetic fault with respect to the main listric normal fault plane. The structural configuration of the spreading end-member and the development of listric faults were investigated previously through experimental (e.g., (Merle and Borgia, 1996)) and numerical models (e.g., (Morgan, 2006)), and compares well to the herein presented structural architecture. Moreover, the observed linkage of the listric landslide fault with the antithetic normal fault (see Fig. 5) is in line with studies of listric fault planes in extensional settings and fault-controlled rollover anticlines (Song and Cawood, 2001).

The second set of end-member models simulated pure rifting (Fig. 5B), achieved by forceful intrusions into the flank. The intrusions of silicone reach from the volcano base to the near-surface (10 cm high within an 11 cm high edifice), thus attempting to represent a near-complete rift dilatation model. Outward-directed displacement is now affecting the entire flank. The rotational shear data, however, reveal that the internal flank itself is not subject to pronounced deformation or shearing. Displacement is rather accomplished by the formation of a basal detachment fault together with thrusts and folds at the outer edge of the flank. Consequently, the forceful intrusion pushes the flank, which is outwardly displaced as a coherent block.

In separate experiments, the depth of the silicone intrusion was varied (downdip limit of intrusion at 4, 6 and 8 cm above the base, see Fig. 6). A similar characteristic pattern was found in all of these experiments independent of the depth of the intrusion. From the top of the intrusion, a set of ~40° inward-dipping normal faults develops, forming a half-graben. From the bottom of the intrusion, a subhorizontal detachment fault inwardly or outwardly dipping up to 10° develops, initiating near the intrusion and propagating outwards towards the free surface. During the experiments, steepening and bulging of the flank occurs as the silicone intrudes, which in some experiments provoked near-surface slumps.

5.2. Combined spreading and rifting

Combined experiments were designed to analyze the feedback between gravitational spreading and rifting, with the main aim being to investigate structural interactions between these two end-member mechanisms. We show deep intrusions only, i.e. silicone intrusions that originate at the base of the half-topographic flank in our model, which in accordance with Walker (1992) and magma intrusions in rift zones. In order to investigate the two-way feedback of spreading and rifting structures, we follow the evolution of two main experiments: (a) a volcano subjected to initial rift zone intrusions that is increasingly influenced by gravitational spreading, and (b) a volcano that is gravitationally spreading into which forceful rift zone intrusions occur.

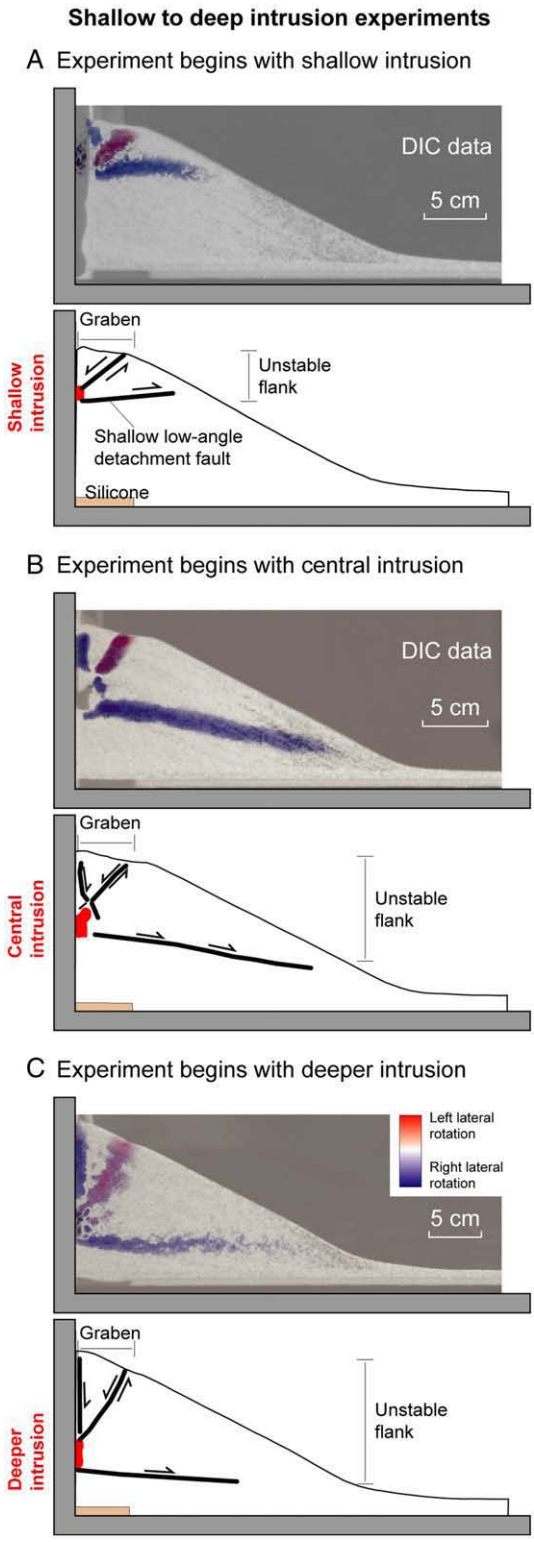

Fig. 6. Experiment showing the effect of the depth of rift zone intrusions, illustrated for A) a shallow intrusion (8 cm), B) a central intrusion (6 cm) and C) a deeper intrusion (4 cm above the base of the model) in a non-spreading flank. Developing structures are a shallow low-angle detachment fault at the bottom of the silicone intrusion, and a graben on top. The structures are generally very similar; though change their position depending on the depth of the silicone intrusion. The presence of a proximal (deep) decollement had no detectable effect on the results.

Fig. 7 shows a volcano model subject to initial forceful intrusions and later gravitational spreading. The half-topographic ridge is laterally pushed by the silicone intrusion and is displaced as a coherent block. Rotational shear data shows a set of ~45° inward-dipping

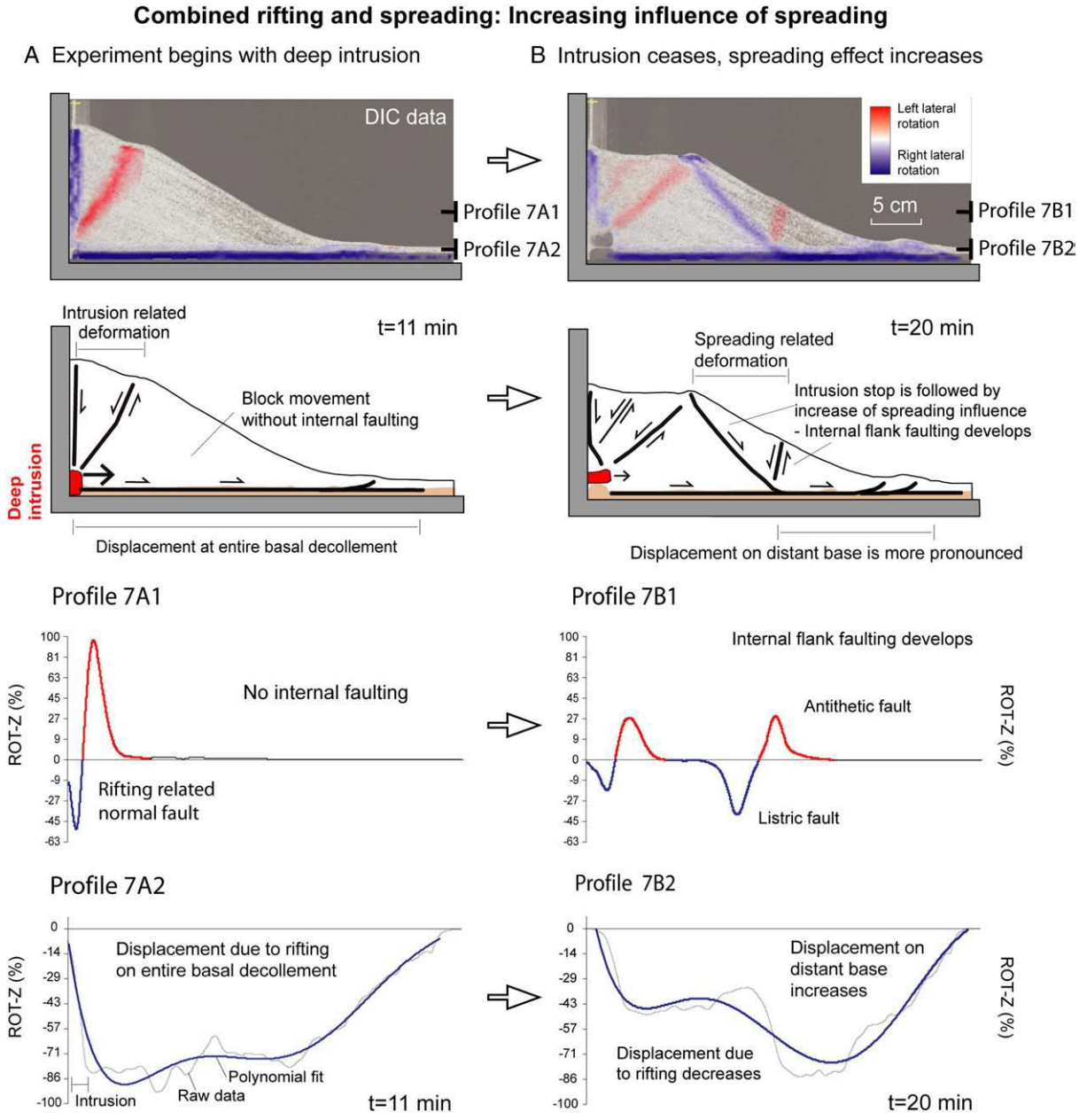

Fig. 7. Experiment showing the combined processes of rifting and spreading, with increasing influence of spreading (i.e. decreasing influence of rift push). Left side (A): Deep rift zone intrusions were simulated and cause a graben on top of the intrusion, basal decollement faulting, and lateral movement of the entire flank. Upper images show DIC results, lower images show interpretation. Profiles 7A1 and 7A2 show normalized amount of rotational shear Z, inside and at the base of the flank. Right side (B): After $t = 15$ min the silicone intrusion was stopped so that the relative effect of spreading increases. New structures develop defining a spreading flank, with a listric and an antithetic normal faults. The rotational shear at the proximal decollement decreases, as does the activity of the graben faults. Profiles 7B1 and 7B2 show a generally increased complexity and non-uniform rotational shear within the flank.

normal faults above the intrusion, as well as dextral fault locations at the basal decollement. In the periphery, a fold and thrust region develops at the flank toe. More details about the location and slip distribution across and along these faults can be seen in the profiles of Fig. 7. The profiles are showing the non-uniform strain rate along the decollement fault that is partly related to fault interaction.

During deep intrusion, the half-graben normal faults above the intrusion and the basal decollement are the only types of faulting, while the moving flank does not experience any internal shear strain (profile 7A1). The decollement displacement is largest near the deep intrusion, with the amount of shear decreasing with distance (profile 7A2). Thus, the first stages of the experiment develop structures similar to those described in earlier end-member models (Fig. 5B). At time $t = 15$ min, the silicone intrusion is stopped by closing the tank trapdoor. As a consequence, the relative importance of spreading increases, so that new structures develop. The changing structural architecture and increasing complexity of flank internal faults are shown in Fig. 7B. Faults that newly form are a listric ~42° outward-dipping normal fault linked to the basal decollement, which is similar to the end-member fault in spreading end-member experiments (Fig. 5A). The flank is experiencing rotational shear localizations at several places, with the faults being active both clockwise and counter-clockwise (profiles 7B1 and 7B2). We note that while spreading is ongoing, the intrusion continues to passively deform associated with half-graben subsidence above. The fault displacements cease; most of the displacement now occurs along the outward-dipping listric normal fault. An inward-dipping antithetic fault develops (74° dip) within the spreading flank, initiating near the kink that connects the decollement and the main normal fault, and propagates upwards. The strain rate at the basal decollement clearly shows the variable slip associated with linking faults.

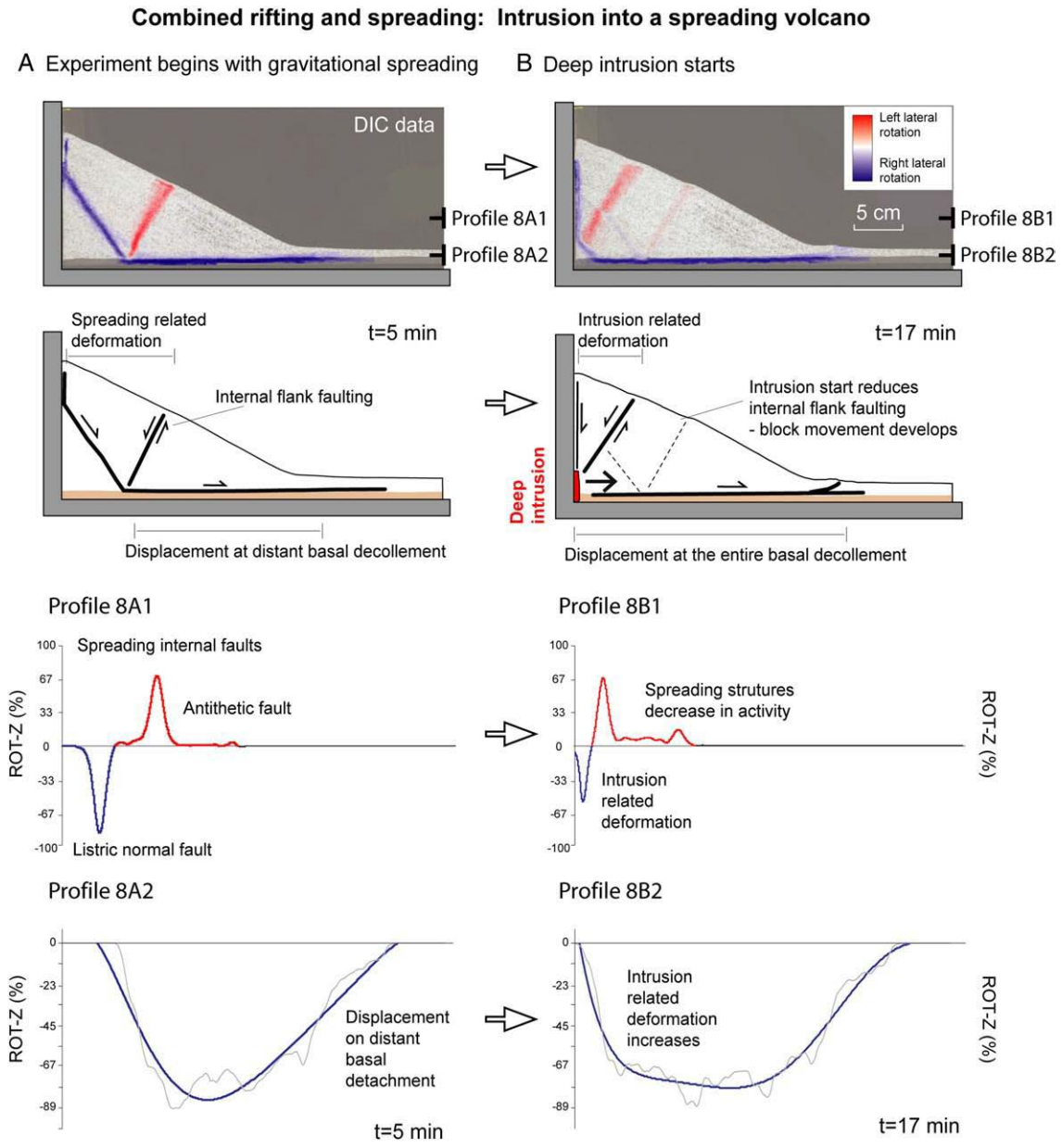

Fig. 8. Experiment showing the combined processes of rifting and spreading, with increasing influence of intrusion. Left side (A): Gravitational spreading causes shear localization at the basal decollement and its listric continuation, connected to an antithetic fault. Profiles 8A1 and 8A2 show rotational shear affecting the internal flank, and the distal part of the decollement. Right side (B): With opening of the trap-door deep rift zone intrusions are simulated. Old structures hindered are the listric and the antithetic normal fault. New structures develop on top of the silicone intrusion and at the proximal part of the deep decollement. Profiles 8B1 and 8B2 show less shear occurring within the flank, but an increased amount of rotational shear at the decollement.

Fig. 8 shows a volcano model subject to gravitational spreading into which forceful intrusions occur. The flank first spreads on top of a weak basal decollement, and develops typical spreading structures, with a basal decollement connected with a 50° outward-dipping listric normal fault and a set of steeply inward-dipping antithetic faults (~70° dip). Rotational shear affects the moving flank, with clockwise and counter-clockwise maxima at the main faults (profile 8A1). Rotational shear at the basal decollement (profile 8A2), is suggesting shear velocities decreasing with distance from the rift zone. After time $t = 15$ min, the trapdoor of the tank is opened to create an intrusion (Fig. 8B). The structural architecture shown by rotational shear changes as soon as the silicone intrudes. The silicone intrusion creates a new 30° inward-dipping normal fault that defines a half-graben above the intrusion. The outward-dipping listric and antithetic normal faults of the spreading flank, in turn, become almost completely inactive. The normalized amount of rotational shear shows that internal shearing within the flank generally decreases (profile 8B1); while at the decollement it is significantly increasing close to the intrusion (profile 8B2). A small step in the shear rate at the decollement matches the location of fault linkage with the listric and antithetic normal faults. With further forceful rift zone intrusion these spreading-structures become completely inactive.

6. Discussion

The size and dynamics of gravitationally spreading volcano flanks are thought to be influenced or even controlled by the presence and architecture of active rift zones (Nakamura, 1980). Through analogue experiments we jointly simulate rift zone intrusions and gravitational spreading, and particularly consider the structural interplay of these two mechanisms. The experiments show how these mechanisms affect mobility and internal deformation of a volcanic flank.

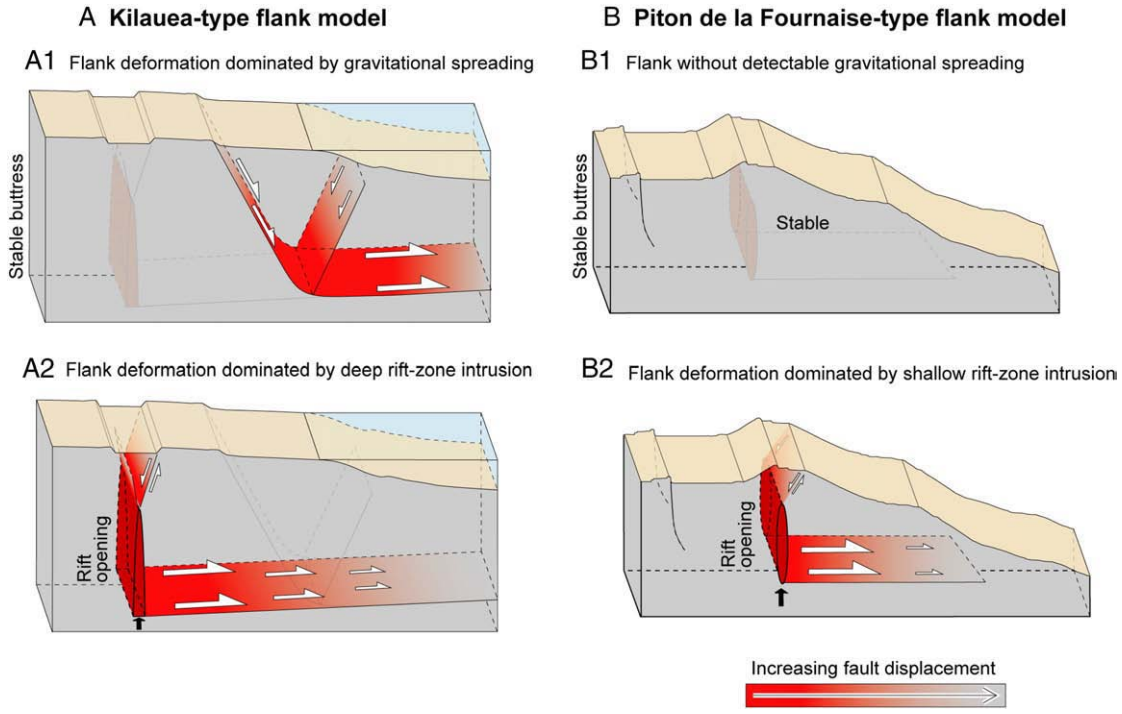

Fig. 9. Sketch illustrating how the results of the experiments may apply to the case scenarios at Kilauea and Piton de la Fournaise. A. The Kilauea-type flank model, here shown for a gravitationally spreading flank. A1. The location of the main listric fault may approximate the Hilina Fault System at the surface. Spreading velocity is highest at the basal decollement and increases at the junction to the antithetic normal fault. A subaerial surface expression of the anthitetic normal fault is not known on Kilauea, though appears to be a geometric necessity in our experiments. A2. Upon forceful opening of the rift zone the activity at the existing faults change, now focussing at the proximal part of the deep decollement and graben subsidence above the rift zone. B. The Fournaise-type flank model is illustrated herein for a conditionally stable flank. B.1 The flank is not moving. B2. Upon intrusion into the rift zone, a detachment fault develops, propagating at shallow dips towards the free flank. Red colors indicate fault zones, for illustration being held in intense red color for high displacements. On both volcano types, a stable buttress causes displacement mainly established on the free flank. See text for details.

6.1. Comparisons of experiments to Kilauea and Piton de la Fournaise

Considering spreading and rifting episodes at the examples of Kilauea and Piton de la Fournaise allows us to re-evaluate some of the structural data and compare them to the variously active fault structures found in experiments. A compilation of the experimental results and application to the two case examples is given in Fig. 9, epitomizing possible modes of volcano spreading and fault interaction influenced by rift zone intrusions.

6.1.1. Kilauea volcano, Hawaii

Various activity periods of Kilauea show similarities to our end-member models. Transitions in the style of deformation at Kilauea occurred between the periods 1934–52, 1952–1983 and 1983–now, associated with changes in magma flux and/or flank spreading (Swanson et al., 1976; Delaney and Denlinger, 1999; Dieterich et al., 2003).

Pure gravitational spreading in Kilauea might concur with periods of less magmatic activity. A period of quiescence without any eruption reports occurred from 1934–1952 (Klein, 1982), during which flank displacement was constrained by a triangulation network and interpreted to be mainly due to flank slip (Swanson et al., 1976). The rate of displacement near the rift zone was low during this period; the so-called *Panau* station moved seaward at an average of only 4–5 cm/yr, about 5–10 times slower than its current rate. Analogue experiments of pure spreading (Figs. 5A and 8A) suggest that flank movement is accommodated by a normal fault connected to the decollement in a listric way. Displacement at the decollement near the base of the rift zone is minor, as recorded by seismic activity at Kilauea during this period. Spreading faults in experiments have their largest displacements at depth. Also, active faults on the south flank of Kilauea are thought to have propagated upward (Peacock and Parfitt, 2002; Holland et al., 2006; Kaven and Martel, 2007).

From 1976 to 1983, activity at Kilauea was predominantly intrusive (Dzurisin et al., 1984), suggesting a possible change from a spreading- to a rifting-dominated volcano. This situation is comparable to our experiment simulating spreading with an increasing influence of intrusion (Fig. 8). Geophysical and petrological observations at Kilauea (Delaney et al., 1990; Gillard et al., 1996) suggest that many of the intrusions traversed almost the entire rift zone, extending from 10 km at the base of the rift up to 3 km below surface. Geodetic data reveal a generally high horizontal displacement rate of the south flank of up to 40 cm/yr (Delaney and Denlinger, 1999). During this intrusion-dominated period, the summit area was dilated and affected by subsidence, while the south flank was under compression associated with localized uplift of up to 2.5 cm/yr (Cayol et al., 2000). In our intrusion end-member model (Fig. 5B), the flank is pushed outwardly by the silicone, also causing subsidence above the intrusion, flank steepening and lateral flank movement. Active faults observed in experiments are graben-conjugate faults originating from the top of the intrusion propagating to the surface, as well as subhorizontal decollement faulting originating at the bottom of the intrusion. The experimental structures thus may compare to the Koae fault system and the decollement at the Kilauea base, both of which were active during the observation period (Duffield, 1975; Delaney et al., 1993). This was also evident from higher seismicity with an average of 250 events $M \geq 2$ per year (Delaney and Denlinger, 1999), occurring mainly on the decollement surface (Gillard et al., 1996). Since 1983, the scale of intrusions has been changing again, now many being located shallow and associated with changes in fault activity and seismicity (Wallace and Delaney, 1995; Delaney et al., 1998). It was even suggested that some intrusions are associated with a reduction in seismicity (Delaney et al., 1998). Our experiments suggest that the scale and shear rates at pre-existing faults strongly depends on the occurrence, dimension and location of intrusions (Figs. 6–8).

Considering the experimental results, we can conjecture that as long as intrusive activity is shallow, the flank is internally subject to fault activity. In this case, proximal decollement slip and seismicity close to the deep rift is limited. A period of deep intrusions may abruptly change this system and cause pronounced and wide subsidence of the rift and reactivate deep decollement seismicity and coherent block movement. Recent research on silent slip events at Kilauea confirms the idea that deep intrusions may cause subsidence at the surface together with pronounced flank movement and proximal (deep) seismicity (Brooks et al., 2008).

6.1.2. Piton de la Fournaise, La Réunion

Piton de la Fournaise is often thought to be structurally similar to Kilauea, although new studies suggest that the mechanism of deformation and shear localization may be very different (Letourneur et al., 2008). Piton de la Fournaise shows two rift zones subject to intrusions, but evidence of lateral flank spreading exists only for short and intermittent periods. Intrusions at Piton de la Fournaise only occur in the shallow part of the edifice, generally ~2 km below the surface (Peltier et al., 2007). This scenario of forceful intrusion may be comparable to our analogue model of a shallow intrusion in a non-spreading flank (Fig. 6). Seismicity at Piton de la Fournaise is mainly located beneath the summit caldera; only very few events occur a kilometer away from the intrusions and may be associated with fault slip at a depth of ~3 km below the surface (Battaglia et al., 2005). In experiments, typical deformation at the surface is subsidence above the intrusion together with the formation of a subhorizontal detachment originating from the bottom of the intrusion. This detachment, although hitherto not clearly identified at Piton de la Fournaise, may be episodically activated. New space geodetic data from Piton de la Fournaise suggest that this decollement may have been active during the 2007 eruptions, associated with a large flank movement event (Froger et al., 2008). Because gravitational spreading alone is less expressed, flank deformation is probably related to rift push and intermittent slip of the flank as a coherent block, as suggested in our experiments. Therefore, we expect the amount of internal shear and development of listric and antithetic normal faults to be minimal at Piton de la Fournaise.

7. Summary and conclusions

Volcanoes are known to interact with basement faults on different scales, affecting the morphology, intrusion geometry, vent distribution and edifice failure (Tibaldi and Lagmay 2006). Large ocean island flanks are subject to deformation associated with combined and interacting processes of gravitational spreading and rift zone intrusions. We designed analogue models to simulate the interaction of associated structures and analyzed them through the DIC method to obtain high resolution strain rates. The results provide new insights about the internal deformation of volcanic flanks. Our interpretation of the models permits us to distinguish two characteristics of flank internal faulting, and demonstrates the modes of structural coupling and fault interaction. Depending on the location and importance of rifting or spreading, different faults may become active or stall, which helps to explain deformation and seismicity changes observed in the two case examples, Kilauea and Piton de la Fournaise.

In end-member models (Fig. 5), we found that: (a) Gravitational spreading is characterized by a destabilization of the flank along a listric normal fault, together with the formation of one or more antithetic normal faults dipping towards the edifice. Thus, the internal flank is subject to rotational shear and structural destabilization. (b) Forceful intrusions in a rift zone are characterized (independent of dike intrusion depth and height) by a sub-horizontal detachment fault originating at the bottom of the intrusion and one or several normal faults that form a structural graben originating at the upper limit of the intrusion. The depth of the subhorizontal detachment and the width of the graben are mainly controlled by the depth of the active rift zone dike intrusion. The unbuttressed flank is pushed as a coherent block.

Experiments combining forceful silicone intrusion and gravitational spreading show that existing fault structures may become locked or activated, depending on the relative influence of dike intrusion and spreading. For instance, a spreading flank that shows active listric and antithetic normal faulting may experience complete locking of these faults during episodes of forceful rift intrusions, while displacement at the basal decollement accelerates. On the other hand, a flank that is subject to a reduced intrusion rates will increasingly develop spreading structures, including listric and antithetic normal faulting. Taken forward to real spreading and rifting volcanic islands, our work suggests that an edifice subject to repeated episodes of rifting and intermittent periods of flank slip may display displacements controlled by faults that appear to dynamically alter their location, strike, dip and rake. These results may help to better understand observations at well-studied volcanoes such as at Kilauea or Piton de la Fournaise.

Acknowledgments

We would like to thank Joel Ruch, Matthias Roseneau and Thomas Ziegenhagen for helping with the experimental setup and PIV technique, and Nina Kukowski and Onno Oncken for continuous lab access and support. Financial aid was provided by the Deutsche Forschungsgemeinschaft through an Emmy Noether Research Grant to TRW (WA 1642/1-4). Constructive reviews by Adelina Geyer, Laurent Michon, and Joan Marti are greatly appreciated.

References

Acosta, J., Uchupi, E., Smith, D., Munoz, A., Herranz, P., Palomo, C., Llanes, P., Ballesteros, M., Carbo, A., Munoz Martin, A., Martin Davila, J., Catalan, M., Marin, J.A., Perez Carrillo, F., Mate, C., 2003. Comparison of volcanic rifts on La Palma and El Hierro, Canary Islands and the Island of Hawaii. Marine Geophysical Researches 24 (1–2), 59–90.

Adam, J., Urai, J.L., Wieneke, B., Oncken, O., Pfeiffer, K., Kukowski, N., Lohrmann, J., Hoth, S., van der Zee, W., Schmatz, J., 2005. Shear localisation and strain distribution during tectonic faulting—new insights from granular-flow experiments and high-resolution optical image correlation techniques. Journal of Structural Geology 27 (2), 283–301.

Adrian, R.J., 2005. Twenty of particle image velocimetry. Experiments in Fluids 39, 159–169.

Annen, C., Lénat, J.F., Provost, A., 2001. The long-term growth of volcanic edifices: numerical modelling of the role of dyke intrusion and lava-flow emplacement. Journal of Volcanology and Geothermal Research 105 (4), 263–289.

Battaglia, J., Ferrazzini, V., Staudacher, T., Aki, K., Cheminée, J.L., 2005. Pre-eruptive migration of earthquakes at the Piton de la Fournaise volcano (Réunion Island). Geophysical Journal International 161 (2), 549–558 (10).

Binard, N., Hékinian, R., Cheminée, J.-L., Searle, R.C., Stoffers, P., 1991. Morphological and structural studies of the Society and Austral hotspot regions in the South Pacific. Tectonophysics 186, 293–312.

Borgia, A., Treves, B., 1992. Volcanic plates overriding the ocean crust: structure and dynamics of Hawaiian volcanoes. In: Parson, L.M., et al. (Ed.), Ophiolites and their modern oceanic analogues. Geological Society London; Special Publication, vol. 60, pp. 277–299.

Borgia, A., 1994. Dynamic basins of volcanic spreading. Journal of Geophysical Research, B, Solid Earth and Planets 99 (9), 17,791–17,804.

Borgia, A., Delaney, P.T., Denlinger, R.P., 2000. Spreading volcanoes. Annual Review of Earth and Planetary Sciences 28, 539–570.

Brenguier, F., Shapiro, N.M., Campillo, M., Nercessian, A., Ferrazzini, V., 2007. 3-D Surface Wave Tomography of the Piton de la Fournaise Volcano Using Seismic Noise Correlations.

Briole, P., Bachèlery, P., McGuire, B., Moss, J., J.-C., R., Soubrault, P., 1998. Deformation of Piton de la Fournaise: evolution of the monitoring techniques and knowledge acquired in the last five years. The European laboratory volcanoes, Proceedings of the second workshop Santorini Greece 2 to 4 May 1996, pp. 467–474.

Brooks, B.A., Foster, J., Sandwell, D., Wolfe, C.J., Okubo, P., Poland, M., Myer, D., 2008. Magmatically triggered slow slip at Kilauea volcano, Hawaii. Science 321, 1177. doi:10.1126/science.1159007.

Carracedo, J.C., 2000. Growth, structure, instability and collapse of Canarian volcanoes and comparisons with Hawaiian volcanoes. Journal of Volcanology and Geothermal Research 94 (1–4), 1–19.

Cayol, V., Dieterich, J.H., Okamura, A.T., Miklius, A., 2000. High magma storage rates before the 1983 eruption of Kilauea, Hawaii. Science 288 (5475), 2343–2346.
Clague, D.A., Denlinger, R.P., 1994. Role of olivine cumulates in destabilizing the flanks of Hawaiian volcanoes. Bulletin of Volcanology 56 (6–7), 425–434.
Delaney, P.T., Denlinger, R.P., 1999. Stabilization of volcanic flanks by dike intrusion: an example from Kilauea. Bulletin of Volcanology 61 (6), 356–362.
Delaney, P.T., Fiske, R.S., Miklius, A., Okamura, A.T., Sako, M.K., 1990. Deep magma body beneath the summit and rift zones of Kilauea Volcano, Hawaii. Science 247 (4948), 1311–1316.
Delaney, P.T., Miklius, A., Arnadottir, T., Okamura, A.T., Sako, M.K., 1993. Motion of Kilauea volcano during sustained eruption from the Puu Oo and Kupaianaha vents, 1983–1991. Journal of Geophysical Research 98 (B10), 17,801–17,820.
Delaney, P.T., Denlinger, R.P., Lisowski, M., Miklius, A., Okubo, P.G., Okamura, A.T., Sako, M.K., 1998. Volcanic spreading at Kilauea, 1976–1996. Journal of Geophysical Research B: Solid Earth 103 (B8), 18003–18023.
Delcamp, A., van Wyk de Vries, B., James, M.R., 2008. The influence of edifice slope and substrata on volcano spreading. Journal of Volcanology and Geothermal Research 177 (4), 925–943.
Denlinger, R.P., Okubo, P., 1995. Structure of the mobile south flank of Kilauea Volcano, Hawaii. Journal of Geophysical Research 100 (B12), 24,499–24,507.
Desmarais, E.K., Segall, P., 2007. Transient deformation following the 30 January 1997 dike intrusion at Kilauea volcano, Hawai'i. Bulletin of Volcanology 69, 353–363.
deVoogd, B., Palomé, S.P., Hirn, A., Charvis, P., Gallart, J., Rousset, D., Danobeitia, J., Perroud, H., 1999. Vertical movements and material transport during hotspot activity: seismic reflection profiling off shore La Réunion. Journal of Geophysical Research 104, 2855–2874.
Dieterich, J., 1988. Growth and persistence of Hawaiian volcanic rift zones. Journal of Geophysical Research 93, 4258–4270.
Dieterich, J.H., Cayol, V., Okubo, P., 2003. Stress changes before and during the Pu'u 'O'o-Ku paianaha eruption. US Geological Survey Professional Paper —(1676), pp. 187–201.
Donnadieu, F., Merle, O., 1998. Experiments on the indentation process during cryptodome intrusions: new insights into Mount St. Helens deformation. Geology 26 (no. 1), 79–82.
Donnadieu, F., Kelfoun, K., van Wyk de Vries, B., Cecchi, E., Merle, O., 2003. Digital photogrammetry as a tool in analogue modelling; applications to volcano instability. Journal of Volcanology and Geothermal Research 123 (1–2), 161–180.
Duffield, W.A., 1975. Structure and origin of the Koae fault system, Kilauea volcano, Hawaii. US Geological Survey Professional Paper 856, 12.
Dvorak, J., 1994. An earthquake cycle along the south flank of Kilauea Volcano, Hawaii. Journal of Geophysical Research 99 (B5), 9533–9541.
Dzurisin, D., Koyanagi, R.Y., English, T.T., 1984. Magma supply and storage at Kilauea volcano, Hawaii, 1956–1983. Journal of Volcanology and Geothermal Research 21, 177–206.
Fiske, R.S., Jackson, E.D., 1972. Orientation and growth of Hawaiian volcanic rifts: the effect of regional structure and gravitational stresses. Proceedings of the Royal Society of London. Series A 329, 299–326.
Froger, J.L., Fukushima, Y., Briole, P., Staudacher, T., Souriot, T., Villeneuve, N., 2004. The deformation field of the August 2003 eruption at Piton de la Fournaise, Reunion Island, mapped by ASAR interferometry. Geophysical Research Letters 31, L14601. doi:10.1029/2004GL020479.
Froger, J.L., Fukushima, Y., Tinard, P., Cayol, V., Souriot, T., Mora, O., Staudacher, T., Durand, P., Fruneau, B., Villeneuve, N., 2008. Multi sensors InSAR monitoring of volcanic activity: the February & April 2007 eruption at Piton de la Fournaise, Reunion Island, imaged with Envisat-ASAR and Alos-PalSAR data. Rapport ESA.
Fukushima, Y., Cayol, V., Durand, P., 2005. Finding realistic dike models from interferometric synthetic aperture radar data: the February 2000 eruption at Piton de la Fournaise. Journal of Geophysical Research 110 (B3), B03206.1–B03206.15.
Gillard, D., Rubin, A.M., Okubo, P., 1996. Highly concentrated seismicity caused by deformation of Kilauea's deep magma system. Nature 384 (6607), 343–346.
Got, J.-L., Fréchet, J., Klein, F.W., 1994. Deep fault plane geometry inferred from multiplet relative relocation beneath the south flank of Kilauea. Journal of Geophysical Research 99 (B8), 15375–15386.
Got, J.-L., Monteiller, V., Monteux, J., Hassani, R., Okubo, P., 2008. Deformation and rupture of the oceanic crust may control growth of Hawaiian volcanoes. Nature 451, 453–456. doi:10.1038/nature06481.
Grujic, D., Walter, T.R., Gartner, H., 2002. Shape and structure of (analogue models of) refolded layers. Journal of Structural Geology 24 (8), 1313–1326.
Holland, M., Urai, J.L., Martel, S., 2006. The internal structure of fault zones in basaltic sequences. Earth and Planetary Science Letters 248 (1–2), 301–315.
Hoth, S., Hoffmann-Rothe, A., Kukowski, N., 2007. Frontal accretion: an internal clock for bivergent wedge deformation and surface uplift. Journal of Geophysical Research 112, B06408. doi:10.1029/2006JB004357.
Hubbert, M.K., 1937. Theory of scale models as applied to the study of geologic structures. Geological Society of America Bulletin 48, 1459–1520.
Johnson, D.J., 1995. Molten core model for Hawaiian rift zones. Journal of Volcanology and Geothermal Research 66 (1–4), 27–35.
Kaven, J.O., Martel, S.J., 2007. Growth of surface-breaching normal faults as a three-dimensional fracturing process. Journal of Structural Geology 29, 1463–1476.
Klein, F.W., 1982. Patterns of historical eruptions at Hawaiian volcanoes. Journal of Volcanology and Geothermal Research 12, 1–35.
LaVision, 2002. StainMaster Manual for DaVis 6.2. LaVision GmbH, Goettingen.
Lénat, J.-F., Labazuy, P., 1990. Morphologies et structures sous-marines de la Reunion. In: Lénat, J.F. (Ed.), Le volcanisme de la Réunion, Monographie. Cent. Rech. Volcanol., Clermont-Ferrand, France(Clermont-Ferrand, France), pp. 43–74.
Lénat, J.-F., Vincent, P., Bachelery, P., 1989. The off-shore continuation of an active basaltic volcano: Piton de la Fournaise (Reunion Island, Indian Ocean); structural and geomorphological interpretation from Sea Beam mapping. Journal of Volcanology and Geothermal Research 36 (1–3), 1–36.
Lénat, J.-F., Gibert-Malengreau, B., Galdéano, A., 2001. A new model for the evolution of the volcanic island of la Réunion (Indian Ocean). Journal of Geophysical Research 106, 8645–8663.
Letourneur, L., Peltier, A., Staudacher, T., Gudmundsson, A., 2008. The effects of rock heterogeneities on dyke paths and asymmetric ground deformation: the example of Piton de la Fournaise (Réunion Island). Journal of Volcanology and Geothermal Research 173 (3), 289–302.
Lipman, P.W., 1980. Rates of volcanic activity along the southwest rift zone of Mauna Loa Volcano, Hawaii. Bulletin of Volcanology 43 (4).
Lipman, P.W., Sisson, T.W., Coombs, M.L., Calvert, A.T., Kimura, J.I., 2006. Piggyback tectonics; long-term growth of Kilauea on the south flank of Mauna Loa. Journal of Volcanology and Geothermal Research 151 (1–3), 73–108.
Lohrmann, J., Kukowski, N., Adam, J., Oncken, O., 2003. The impact of analogue material properties on the geometry, kinematics, and dynamics of convergent sand wedges. Journal of Structural Geology 25 (10), 1691–1711.
Longpré, M.-A., Staudacher, T., Stix, J., 2007. The November 2002 eruption at Piton de la Fournaise volcano, La Réunion Island: ground deformation, seismicity, and pit crater collapse. Bulletin of Volcanology 69, 511–525. doi:10.1007/s00445-006-0087-0.
Merle, O., Borgia, A., 1996. Scaled experiments of volcanic spreading. Journal of Geophysical Research, B, Solid Earth and Planets 101 (6), 13,805–13,817.
Merle, O., Lénat, J.-F., 2003. Hybrid collapse mechanism at Piton de la Fournaise volcano, Reunion Island, Indian Ocean. Journal of Geophysical Research 108 (B3), 2166. doi:10.1029/2002JB002014.
Michon, L., Saint-Ange, F., 2008. Morphology of Piton de la Fournaise basaltic shield volcano (La Re'union Island): characterization and implication in the volcano evolution. Journal of Geophysical Research 113, B03203. doi:10.1029/2005JB004118.
Michon, L., Saint-Ange, F., Bachelery, P., Villeneuve, N., Staudacher, T., 2007. Role of the Structural Inheritance of the Oceanic Lithosphere in the Magmato-Tectonic Evolution of Piton de la Fournaise Volcano (La Reunion Island).
Mitchell, N.C., 1998. Characterising the irregular coastlines of volcanic ocean islands. Geomorphology 23 (1), 1–14.
Moore, J.G., Krivoy, H.L., 1964. The 1962 flank eruption of Kilauea volcano and structure of the East Rift Zone. Journal of Geophysical Research 69, 2033–2045.
Moore, J.G., Chadwick, W.W., 1995. Offshore geology of Mauna Loa and adjacent areas, Hawaii. In: Rhodes, J.M., Lockwood, J.P. (Eds.), Mauna Loa Revealed: Structure, Composition, History, and Hazards, American Geophysical Union, Washington, D.C., pp. 21–44.
Morgan, J.K., 2006. Volcanotectonic interactions between Mauna Loa and Kilauea; insights from 2-D discrete element simulations. Journal of Volcanology and Geothermal Research 151 (1–3), 109–131.
Morgan, J.K., Clague, D.A., 2003. Volcanic spreading on Mauna Loa volcano, Hawaii: evidence from accretion, alteration, and exhumation of volcaniclastic sediments. Geology 31 (5), 411–414.
Morgan, J.K., Moore, G.F., Hills, D.J., Leslie, S., 2000. Overthrusting and sediment accretion along Kilauea's mobile south flank, Hawaii: evidence for volcanic spreading from marine seismic reflection data. Geology 28 (7), 667–670.
Nakamura, K., 1980. Why do long rift zones develop in Hawaiian volcanoes; a possible role of thick oceanic sediments. Kasan = Bulletin of the Volcanological Society of Japan 25 (4), 255–269.
Oehler, J.F., van, W.d.V.B., Labazuy, P., 2005. Landslides and spreading of oceanic hot-spot and arc shield volcanoes on low strength layers (LSLs); an analogue modeling approach. Journal of Volcanology and Geothermal Research 144 (1–4), 169–189.
Owen, S., Segall, P., Lisowski, M., Miklius, A., Denlinger, R., Sako, M., 2000. Rapid deformation of Kilauea Volcano: Global Positioning System measurements between 1990 and 1996. Journal of Geophysical Research B: Solid Earth 105 (8), 18,983–18,998.
Peacock, D.C.P., Parfitt, E.A., 2002. Active relay ramps and normal fault propagation on Kilauea, Hawaii. Journal of Structural Geology 24, 729–742.
Peltier, A., Ferrazzini, V., Staudacher, T., Bachèlery, P., 2005. Imaging the dynamics of dyke propagation prior to the 2000–2003 flank eruptions at Piton de La Fournaise, Reunion Island. Geophysical Research Letters 32, L22302. doi:10.1029/2005GL023720.
Peltier, A., Staudacher, T., Bachèlery, P., 2007. Constraints on magma transfers and structures involved in the 2003 activity at Piton de La Fournaise from displacement data. Journal of Geophysical Research 112, B03207. doi:10.1029/2006JB004379.
Ramberg, H., 1981. Deformation structures in theory and experiments. In: Symposium on experiment and theory in geology 103; 1. Geological Society of Sweden, Stockholm, Sweden, 131.
Roche, O., Druitt, T.H., Merle, O., 2000. Experimental study of caldera formation. Journal of Geophysical Research 105 (B1), 395–416.
Rubin, A.M., 1990. A comparison of rift-zone tectonics in Iceland and Hawaii. Bulletin of Volcanology 52 (4), 302–319.
Rubin, A.M., 1992. Dike-induced faulting and graben subsidence in volcanic rift zones. Journal of Geophysical Research 97 (B2), 1839–1858.
Rubin, A.M., Gillard, D., 1998. Dike-induced earthquakes: theoretical considerations. Journal of Geophysical Research B: Solid Earth 103 (B5), 10017–10030.
Schellart, W.P., 2000. Shear test results for cohesion and friction coefficients for different granular materials: scaling implications for their usage in analogue modelling. Tectonophysics 324 (1–2), 1–16.
Segall, P., Desmarais, E.K., Shelly, D., Miklius, A., Cervelli, P., 2006. Earthquakes triggered by silent slip events on Kilauea volcano, Hawaii. Nature 442, 71–74.
Sigmundsson, F., Durand, P., Massonnet, D., 1999. Opening of an eruptive fissure and seaward displacement at Piton de la Fournaise volcano measured by RADARSAT satellite radar interferometry. Geophysical Research Letters 26 (5), 533–536.
Song, T., Cawood, P.A., 2001. Effects of subsidiary faults on the geometric construction of listric normal fault systems. AAPG Bulletin 85 (2), 221–232.

Stieltjes, L., Moutou, P., 1989. A statistical and probabilistic study of the historic activity of Piton de la Fournaise, Reunion Island, Indian Ocean. Journal of Volcanology and Geothermal Research 36 (1–3), 67–86.
Swanson, D.A., Duffield, W.A., Fiske, R.S., 1976. Displacement of the south flank of Kilauea Volcano; the result of forceful intrusion of magma into the rift zones. U. S. Geological Survey, Reston, VA, United States, p. 39.
ten Grotenhuis, S.M., Passchier, C.W., Bons, P.D., 2002. The influence of strain localisation on the rotation behaviour of rigid objects in experimental shear zones. Journal of Structural Geology 24 (3), 485–499.
Thurber, C.H., Gripp, A.E., 1988. Flexure and seismicity beneath the south flank of Kilauea Volcano and tectonic implications. Journal of Geophysical Research 93, 4271–4278.
Tibaldi, A., Lagmay, A.M.F., 2006. Preface: interaction between volcanoes and their basement. Journal of Volcanology and Geothermal Research 158 (1–2), 1–5. doi:10.1016/j.jvolgeores.2006.04.011.
van Wyk de Vries, B., Matela, R., 1998. Styles of volcano-induced deformation; numerical models of substratum flexure, spreading and extrusion. Journal of Volcanology and Geothermal Research 81 (1–2), 1–18.
Wada, Y., 1994. On the relationship between dike width and magma viscosity. Journal of Geophysical Research 99 (B9), 17,743–17,755.
Walker, G.P.L., 1986. Koolau Dike Complex, Oahu: intensity and origin of a sheeted-dike complex high in a Hawaiian volcanic edifice. Geology 14 (4), 310–313.
Walker, G.P.L., 1987. The dike complex of Koolau Volcano, Oahu: internal structure of a Hawaiian rift zone. US Geological Survey Professional Paper 1350 (2), 961–993.
Walker, G.P.L., 1988. Three Hawaiian calderas: an origin through loading by shallow intrusions? Journal of Geophysical Research 93 (B12), 14,773–14,784.
Walker, G.P.L., 1992. "Coherent intrusion complexes" in large basaltic volcanoes; a new structural model. Journal of Volcanology and Geothermal Research 50 (1–2), 41–54.
Walker, G.P.L., 2000. Basaltic volcanoes and volcanic systems. In: Sigurdsson, H. (Ed.), Encyclopedia of Volcanoes. Academic Press, New York, pp. 283–289.
Wallace, M.H., Delaney, P.T., 1995. Deformation of Kilauea volcano during 1982 and 1983: a transition period. Journal of Geophysical Research 100 (B5), 8201–8219.
Walter, T.R., Schmincke, H.U., 2002. Rifting, recurrent landsliding and Miocene structural reorganization on NW-Tenerife (Canary Islands). International Journal of Earth Science 91, 615–628.
Walter, T.R., Amelung, F., 2006. Volcano-earthquake interaction at Mauna Loa Volcano, Hawaii. Journal of Geophysical Research.
Walter, T.R., Kluegel, A., Muenn, S., 2006. Gravitational spreading and formation of new rift zones on overlapping volcanoes. Terra Nova 18 (1), 26–33.
White, D.J., Take, W.A., Bolton, M.D., 2001. Measuring soil deformation in geotechnical models using digital images and PIV analysis. 10th International Conference on Computer Methods and Advances in Geomechanics, Tucson, Arizona.